American Mineralogist, Volume 87, pages 1128–1138, 2002

The grid-work texture of authigenic microcrystalline quartz in siliceous crust-type (SCT) mineralized horizons

GIANFRANCO CAMANA,[1,*] DANIEL CHATEIGNER,[2] MICHELE ZUCALI,[2,3] AND GILBERTO ARTIOLI[3,4]

[1]Dipartimento di Ingegneria dei Materiali, Università di Trento, Via Mesiano 77, I-38050 Trento, Italy
[2]Laboratoire de Physique de l'Etat Condensé, Université du Maine, Av. Messiaen, F-72085 Le Mans, France
[3]Dipartimento di Scienze della Terra, Università di Milano, Via Botticelli 23, I-20133 Milano, Italy
[4]Centro CNR di Studio per la Geodinamica Alpina e Quaternaria, Via Mangiagalli 34, I-20133 Milano, Italy

ABSTRACT

Siliceous crust-type (SCT) formations are pervasive silicified horizons associated with fluorite-barite-polymetallic sulfide mineralization in carbonate rocks. They almost invariably show a peculiar grid-work texture formed by microcrystalline quartz. The mineralogical and textural features of several SCT samples from Italy, Spain, France, China, and Brazil were investigated by optical and electron microscopy and X-ray and neutron powder diffraction. The resulting {001} pole figures exhibit two main components of orientation of the crystallographic *c* axis with respect to the normal to the sample surface, one located at about 35° and the other in the range 60–85°. The observed textural features are seen in all samples and they appear to be independent of the age and geographical location of the SCT formation. The observed grid-work texture is tentatively interpreted as forming by nucleation of quartz seeds on specific faces of surrounding crystals. The observed morphology and the regularly oriented populations of crystals are consistent with simultaneous growth of quartz crystals having well-defined reciprocal orientations. The grid-work texture of quartz in SCT horizons is similar to the type reported for Magadi-type cherts, which are commonly interpreted as formed by magadiite-mediated silica precipitation processes. Since the genesis of SCT deposits is totally unrelated to alkaline-lake genetic processes, it is concluded that cherts showing strongly textured patterns of microcrystalline quartz may have a different origin than Magadi-type deposits.

INTRODUCTION

A peculiar grid-work texture of microcrystalline sedimentary quartz has been repeatedly observed during the investigation of pervasively silicified ore-bearing horizons found in the uppermost part of carbonate platform sequences from different geotectonic settings. Typical examples of siliceous crusts overlying carbonate layers are shown in Figure 1. These peculiar horizons have been defined as Siliceous Crust-Type (SCT) mineralizations (Brigo et al. 1988; Rodeghiero et al. 1996; Camana 1999, 2000; Brigo et al. 2001; Camana et al. 2001). They show extensive secondary enrichment in barite, fluorite, and base metal sulfides (Pb-Zn, Sb, Sb-Cu-Hg, and Cu minerals), and may be considered a well-defined class within the known types of carbonate-hosted deposits. The SCT horizons occur with variable thickness (from a few decimeters to some tens of meters), lateral extension up to 100 km at the top of carbonate sequences, and range in age from Proterozoic to Tertiary. SCT deposits are known from the Italian Alps, Sardinia, French and Spanish Pyrenees, China, and Brazil. A literature survey of carbonate-hosted deposits suggests that SCT horizons are also present in the United States, Mexico, South Africa, Kuwait, Tunisia, and Australia (see discussion and references in Camana 1999, and in Brigo et al. 2001).

The present investigation aims to fully characterize the three-dimensional texture of SCT quartz samples from different localities (Table 1) by optical microscopy, scanning electron microscopy, and texture analysis based on X-ray and neutron powder diffraction data. Possible genetic processes producing this peculiar texture, based on the observed features and on the assumed geological constraints of SCT horizons are discussed.

Several previous studies recognized the grid-work texture of microcrystalline quartz in some SCT occurrences, although no full characterization was attempted. McNight and Fischer (1970) found textured quartz in the jasperoid bodies of Picher Field in the Pb-Zn Mississippi Valley Type district (U.S.A.) and they described it as a "prismatic elongation" of the quartz crystals. Isoli (1972) described the microcrystalline quartzitic host rock of an Italian Norian fluorite mineralization in the central southern Alps as characterized by a "grid-pattern" of quartz microcrystals. Magliola-Mundet (1972a, 1972b) described "cross texture" in quartz microcrystals in the silicified and fluorite mineralized bodies of the El Tule district (Mexico). Rodeghiero (1977) studied Middle Triassic silicified stratabound fluorite-bearing bodies of the Presolana Mine (central southern Alps, Italy) and recognized a preferential array of many elongated quartz crystals along two almost perpendicular directions. Lovering and Heyl (1980) reported the presence of a typical "jigsaw puzzle" in the quartzitic groundmass of the jasperoid rocks of the Pando area (Colorado).

* E-mail: artioli@iummix.terra.unimi.it

Other authors observed a grid-work texture in microcrystalline quartz within siliceous rocks derived from different geological environments. Schubel and Simonson (1990) first used the term "rectilinear or grid-work orientation" to describe the groundmass of Pleistocene high-alkali cherts from Lake Magadi, Kenya (Fig. 2a). The authors proposed that the grid-work texture could be inherited from the sodium silicate precursor magadiite [$NaSi_7O_{13}(OH)_3 \cdot 3H_2O$] which displays similar optical extinction patterns. This fact implies a direct volume-by-volume replacement of magadiite by quartz during the chert genesis in an alkaline environment. Following the work of Schubel and Simonson (1990), the petrographic identification of the grid-work texture of quartz in cherts from various geological settings and ranging in age from Pleistocene to Archean has been interpreted as a signature of Magadi-type processes (e.g., Krainer and Spötl 1998). Hattori et al. (1996) found grid-work texture in some domains of bed cherts in a Miocene volcanic-sedimentary succession in Japan (Fig. 2b). In this case, optical microscopic observation under high magnification established that the grid-work pattern was composed of an interlocking aggregation of minute spherules of length-fast chalcedony. The authors did not find magadiite in their samples and assumed that the cherts were the products of devitrification of volcanic ash, extensive pedogenesis, and colloidal accumulation of silica in evaporitic conditions.

GEOLOGICAL FEATURES OF SCT HORIZONS

SCT horizons may be described as silicified lithological units overlying karst-solution landscapes which evolved on carbonate platforms during emergence (Fig. 1). They represent the complete silicification of polymictic conglomerate-breccias made up of carbonate fragments and rare siliciclastic rocks developed on palaeokarst landscapes. No magmatic or volcanic rocks are related to SCT formations. Ubiquitous morphological features are: (1) unconformity-concordant tabular bodies; (2) discordant columnar bodies representative of filled paleofractures and paleofaults. Transgressive siliciclastic sedimens always overlie the SCT horizons.

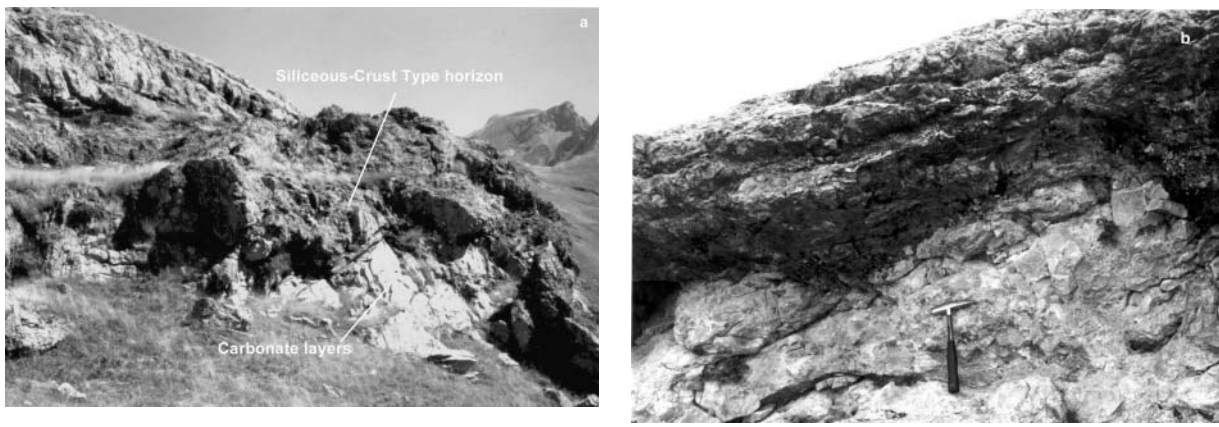

FIGURE 1. (**a**) Example of an SCT horizon (gray) overlying a carbonate substratum (white) at Puerto de Formigal/Pourtalet, Central Pyrenees. (**b**) View of a typically sharp contact between an SCT body and carbonate layers at the Chialderate area in the Carnic Alps, northeast Italy. Both occurrences are Lower Carboniferous in age.

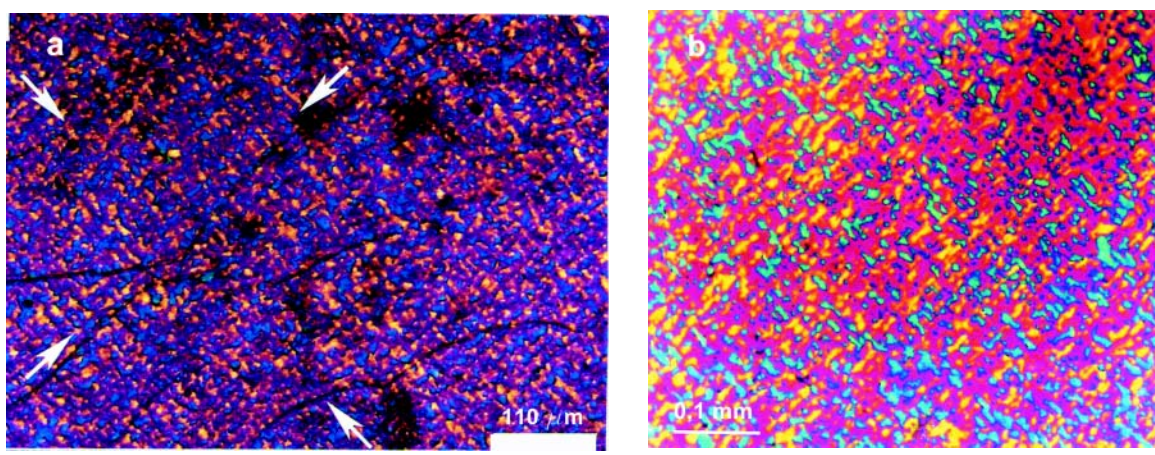

FIGURE 2. (**a**) Groundmass chert form Lake Magadi displaying a rectilinear or grid-work extinction pattern (from Schubel and Simonson 1990). (**b**) Chert nodule showing grid-work texture inside the chert bed of the Miocene Kunimi Formation of central Japan (from Hattori et al. 1996).

TABLE 1. List of localities and geological settings of SCT quartz samples investigated in this work

Geological Setting	Samples	Locality	Main References
Southern central Alps (Lombardy, Italy)	CA1, CA2 BE	Camissinone mine Costa Imagna area	Jadoul et al. (1993) Isoli (1972), Jadoul and De Bonis (1981)
Southern central Alps (Lombardy, Italy)	V2B, GSW, BUDR PRA, PRAA	(Pb-Zn.F-Ba) Gorno District Presolana mine	Assereto et al. (1977) Rodeghiero (1977)
Southern Appennines (Calabria, Italy)	TSA22 TSA21	Timpone Scifarello and Monte Caramolo area	Bonardi et al. (1982)
Palaeocarnic Chain (southern eastern Alps, Italy)	T11, T27, T30B T22IIG, T25IM, T25IA, T25IG, B1, F5S	Southern Monte Coglians and Chialderate area Rio Chianaletta area	Brigo et al. (1988) Rodeghiero et al. (1996) Brigo et al. (2001)
Western Pyrenees (Spanish-French boundary)	PO1 PO2	Puerto de Formigal and Pourtalet mines	Subías et al. (1997, 1998) Subías and Fernández-Nieto (1995)
Western Asturias (Spain)	BERC	Berbes – La Cabaña	Tejerina and Zorrilla (1980), Spiro et al. (1999)
Hunan Province (China)	XIK, XIKV2	Xikuangshan area	Yi et al. (1999)
Central Pyrenées (Spain)	YE	Yenefrito area	Subías et al. (1999)
Central Pyrenées (France)	AS	Arrens area	Pouit and Bois (1986), Pouit (1993)
Southwest Sardinia (Sulcis-Iglesiente, Italy)	MS, MSB, MSC CSC SL1, SL2, SL3	Monte Segarino area Corona Sa Craba area Serra Lurdagu area	Pretti and Tamburrini (1968) Bechstädt et al. (1994)
Chapada Diamantina (Bahia, Brasil)	F2021	Município de Nova Redenção area	Souza et al. (1993)
Bambuí Group (Minas Gerais, Brasil)	MSJ MG	Município de Itacarambí (Mina San João and Grande)	Robertson (1963)

Notes: Selected references for each SCT occurrences are also indicated.

The presence of SCT fragments in the transgressive siliciclastic sediments show that the SCT horizons developed before the siliciclastic sedimentation. Schönlaub and Kreutzer (1993) found that for the SCT horizon in the Mt. Coglians area of the Carnic Alps (Italy), the stratigraphic interval between the end of the paleokarstic event and the beginning of the transgressive siliciclastic sedimentation was no more than few million years (*texanus* and *early bilineatus* zones of the Lower Visean**)**. Therefore, the silicification process in SCT horizons may be a relatively fast geological process. One model of formation of SCT horizons (Camana 1999, Brigo et al. 2001) implies that the silica may be produced during illitization of clay-rich basinal sediments during diagenesis. This assumption is supported by the oxygen isotope composition of SCT microcrystalline quartz ($\delta^{18}O$ values in the range +18.5‰ and +24.6‰, independent of age and geotectonic setting), which is in good agreement with the $\delta^{18}O$ values of authigenic quartz derived from illitization of clay-rich basinal sequences or lagoonal sediments (+18–26‰, Yeh and Savin 1977). The general agreement between the sulfur isotope composition of barites with the $\delta^{34}S_{CDT}$ "age curve" of sulfate of sea water through time, suggests that the source of barite sulfur was ocean water or related brines. Convective hydrologic systems may be responsible for transport and concentration of the silica-rich fluids within the basin (Brigo et al. 2001).

EXPERIMENTAL TECHNIQUES

SEM observations were performed using a Cambridge Stereoscan 250 instrument with a constant accelerating voltage of 20 kV. The samples were mechanically separated from the bulk specimens, then assembled on a slide glass using a graphite-based adhesive and coated with gold.

X-ray powder diffractograms were obtained with a Philips PW1130-PW1050 X-ray powder diffractometer equipped with a Cu tube operated at 40 kV and 40 mA. The data were collected over the angular range 5–50° 2θ. Extraction of the peak profile parameters of quartz (sample broadening) and identification of the mineralogical phases present in each sample were performed using a full-profile Rietveld type analysis. The GSAS software system was employed throughout (Larson and Von Dreele 1999).

X-ray texture analysis of SCT microcrystalline quartz specimens was performed using a CPS120 position-sensitive detector from Inel and a Huber four-circle goniometer, using Cu$K\alpha_{1,2}$ radiation in reflection mode and flat specimens. This methodology allows simultaneous collection of all pole figures in the range $0 < 2\theta < 120°$ for each sample orientation (Ricote et al. 2000). The pole figures are obtained from the numerical direct integration of the available peaks of around 1000 diffraction diagrams corresponding to all measured sample orientations. Once collected, the integrated net intensities are obtained by removing the background, then correcting for absorption and localization (Heizmann and Laruelle 1986) to obtain raw pole figures. The raw pole figures are input for refinement of the Orientation Distribution (ODF) by the WIMV method (Matthies and Vinel 1982a, 1982b), which normalizes the intensities of the raw pole figures into distribution densities, as implemented in the BEARTEX package (Wenk et al. 1998). The distribution

densities are expressed in multiples of a random distribution (m.r.d.). An untextured powder will exhibit all pole figures with homogeneous densities of 1 m.r.d., while pole figures for a textured sample will be reinforced in certain regions, depending on the texture strength. The texture strength is estimated by the texture index, F^2 (Bunge 1982), and the quality of the OD refinement by the reliability factors RP_0 (calculated for all densities of the pole figures) and RP_1 (calculated for densities above 1 m.r.d.) (Matthies et al. 1987). When a satisfactory reliability of the ODF is obtained, it is filtered to avoid grain-size related problems (Matthies et al. 1987), and the pole figures for low Miller indices are calculated.

For microcrystalline quartz (space group $P3_221$, a = 4.912 Å, c = 5.404 Å), we acquired all data for the diagrams with a constant incidence angle $\omega = 13°$, which is approximately half the angle at which the 101 peak occurs, and gives an irradiated area on the sample of approximately 1×5 mm^2. This area was further increased to 5×5 mm^2 by oscillating the sample during acquisition, to probe a larger number of grains. In this configuration, we estimate the number of irradiated grains to be on the order of 10^4. The tilt angle (χ) was varied from 0 to 70° and the azimuthal angle (φ) from 0 to 355°, both in steps of 5°. A counting time of 60 seconds for each diagram provided enough intensity to reliably measure most of the diffracted peaks in the low angle region, as illustrated by Figure 3a.

A similar setup was used at the D1B line of the ILL (France) high-flux reactor to probe a larger specimen volume (1 cm^3). Only two samples were measured. The experiments were done in transmission mode, and absorption corrections are avoided because of the low neutron absorption of quartz. Each of the peaks was fitted with a Gaussian shape for all sample orientations. The wavelength used (2.523 Å) and the detector aperture of 80° limited somewhat the number of available pole figures, but the completeness of each pole figure was increased due to the absence of defocusing (Fig. 3b). Details of the neutron procedure may be found in Chateigner et al. (1997).

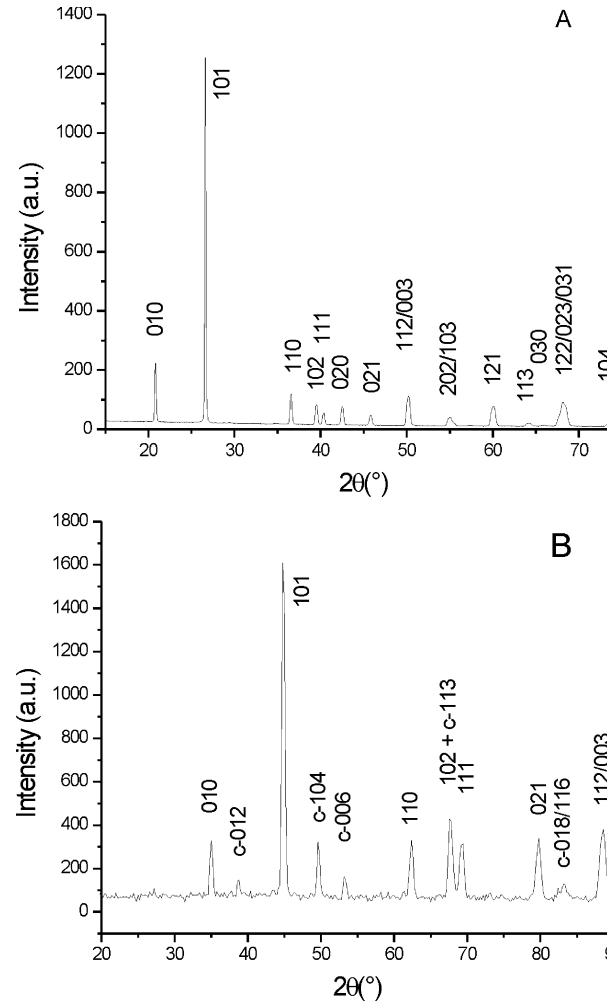

FIGURE 3. Examples of typical X-ray and neutron powder diffraction patterns collected for texture analysis from samples PRAA (**a**) and T11A (**b**). About 1000 such patterns collected at different tilt angles for each sample were used to reconstruct the three-dimensional texture.

DISCUSSION OF THE GRID-WORK TEXTURE BASED ON OPTICAL MICROSCOPY, SEM, AND XRPD

In the SCT horizons the silica is always present as microcrystalline quartz, and no opal or chalcedony have been identified. The average grain size of the quartz crystals is about 50 μm and the horizons invariably show extensive grid-work texture (Figs. 4a–4c). The observed grain size is slightly larger than the average size of 10 μm reported for most cherts (Knauth 1994). The grid-work texture is particularly evident when observed with the gypsum plate inserted in an optical microscope. The quartz crystals describe a regular grid pattern, with two populations of elongated grains arranged in sub-perpendicular directions (i.e., the blue and yellow grains in Figs. 4a–4c). Other more or less elongated grains appear reddish. When the sample stage is rotated by 45° the iso-oriented elongated quartz grains switch alternatively from extinct (red) to light positions (blue and yellow), while the poorly elongated grains almost always remain red. Only in a few limited regions do the quartz microcrystals show a near random distribution or a gradual transition to textured domains (Fig. 4c). There is no straightforward relationship between the presence of the grid-work texture and other mineralogical (i.e., the presence of other mineral phases), chemical, or macroscopic parameters.

Most of the investigated SCT cherts show well-developed grid-work texture. Only in the case of the SCT samples from Calabria (Monte Pollino, southern Italy) and from some localities in the French Pyrenees (Arrens zone) the texture is absent (Fig. 4f). The lack of texture in these samples is related to post-diagenetic metamorphic processes (greenschist facies) that involved the SCT horizons and obscured the original rock features. The recrystallization (and larger grain size) of quartz in these samples may also be indirectly perceived by the substantially lower values of the Lorentzian part (LX) of the peak profile broadening as evidenced by XRPD (Table 2).

Other typical features observed by optical microscopy are as follows:

(1) The grid-work texture is not an inherited feature: in partly silicified fragments of limestone there is the clear presence of

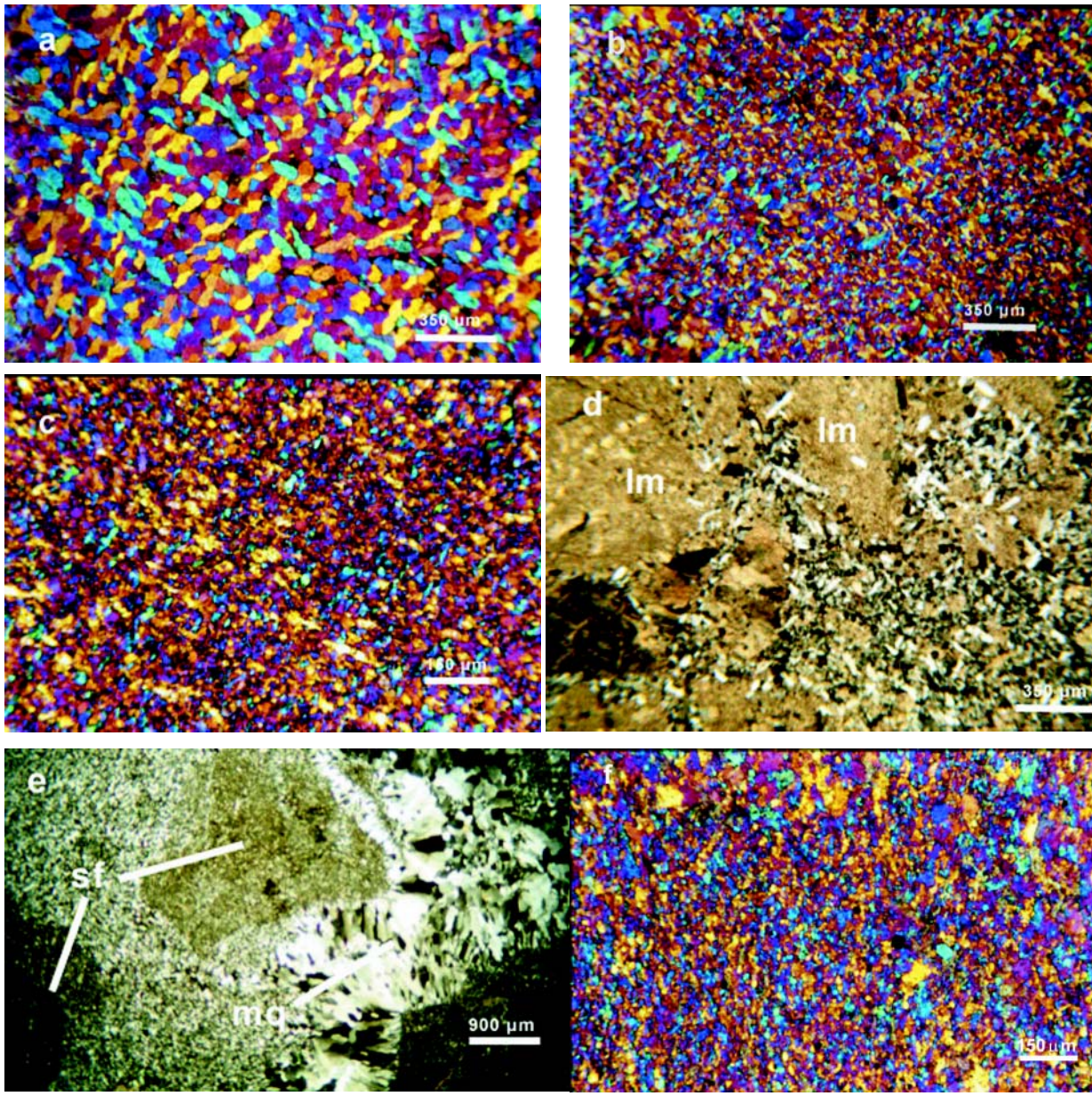

FIGURE 4. Pictures of grid-work textures in SCT cherts obtained by optical microscopy. (**a**) sample B2, crossed polarized light (CPL), gypsum plate inserted (GPI); (**b**) sample PO, CPL, GPI; (**c**) sample PRA, CPL, GPI; (**d**) sample T27, CPL (lm: limestone); (**e**) sample SL, CPL (sf = silicified fragments; mq = macrocrystalline quartz); (**f**) sample AS, CPL. The dimensions of the field of view are indicated by the white bars on each image.

an homogeneous micritic groundmass and no microstructure or texture that may explain the orientation of the quartz grains (Fig. 4d). In many instances microscopic carbonate inclusions within the single quartz crystals can be recognized. They are assumed to be relicts of the original carbonate matrix that survived the silicification process.

(2) The grid-work texture appears very much the same in thin sections cut along different directions of a given oriented sample (for example, parallel, perpendicular, or at an angle to macroscopic layering).

(3) The texture may be formed by quartz grains having different sizes. In rare cases it is possible to recognize within the quartz matrix the original shape of the now-silicified fragments, sometimes having a round shape, formed by quartz grains of different sizes (Fig. 4e).

(4) Macrocrystalline quartz usually occurs in fractures or voids with palisadic and/or mosaic morphologies (Fig. 4e).

Figure 5 shows SEM images of SCT samples from the Upper Triassic Gorno District (northern Italy). Some domains within the Gorno specimens show quartz crystals of unusually

TABLE 2. List of provenance and age of the SCT quartz samples and mineral phases identified by XRPD

Age	Sample	GW	LX	Size (μm)	Phases
			Southern Central Alps (Lombardy, Italy)		
	CA1	12.4	3.89	20.43	quartz, fluorite, phyllosilicates
Norian	CA2	6.9	4.14	19.20	quartz, fluorite
	BE	9.9	3.75	21.20	quartz, fluorite
			Southern Central Alps (Pb-Zn-F-Ba Gorno District, Italy)		
	V2B	14.4	3.43	23.18	quartz
Carnian	GSW	10.7	3.23	24.61	quartz, calcite, fluorite
	BUDR	12.2	4.31	18.44	quartz, hemimorphite, illite
	PRA	10.7	3.81	20.87	quartz, illite
			Calabria (Italy)		
	TSA22	19.1	2.96	26.86	quartz, fluorite, illite
Carnian	TSA21	22.3	4.10	19.39	quartz, barite, illite
			Southern Eastern Alps (Palaeocarnic Chain, Italy)		
	T27	15.2	3.52	22.59	quartz, calcite
	T25IG	14.4	3.85	20.65	quartz, feldspars, illite
Lower	T25IM	15.4	3.63	21.90	quartz
Carboniferous	T30B	16.2	3.57	22.27	quartz, calcite, illite
	F5S	9.7	4.13	19.25	quartz, calcite, illite, sphalerite
	T22IIG	15.0	4.13	19.25	quartz, calcite, feldspars, illite
			Spanish-French Pyrenees (Puerto de Formigal/Pourtalet area)		
Lower	PO1	8.9	3.97	20.03	quartz, fluorite, phyllosilicates
Carboniferous	PO2	8.1	3.80	20.92	quartz, fluorite
			Hunan Province (Xikuangshan area, China)		
Upper	XIK	13.2	4.00	19.88	quartz, calcite, stibnite, kaolinite
Devonian	XIKV2	13.0	3.47	22.91	quartz, calcite, stibnite, illite
			Spanish Pyrenees (Yenefrito area)		
Devonian	YE	9.9	3.92	20.28	quartz, pyrite, galena, illite, kaolin-
ite					
			French Pyrenees (Arrens area)		
Devonian	AS	13.3	2.75	28.91	quartz, pyrite, celsian, arsenopy-
rite, cymrite, bournonite					
			Sardinia (Sulcis-Iglesiente area, Italy)		
	MS	13.3	3.98	19.98	quartz
	MSB	11.6	3.68	21.60	quartz, calcite, feldspars, illite
Lower	MSC	12.9	4.11	19.34	quartz, illite, cerussite
Ordovician	CSC	10.9	3.94	20.18	quartz, barite
	SL1	11.6	3.68	21.60	quartz, dolomite
	SL2	9.3	4.14	19.20	quartz, barite
	SL4	7.7	4.25	18.71	quartz, dolomite, barite, illite
			Brasil (Minas Gerais and Bahia)		
	F2021	14.5	3.86	20.60	quartz, dolomite, pyrite
Upper	MSJ	6.4	4.51	17.63	quartz, sphalerite, galena, fluorite
Proterozoic	MG	8.7	3.77	21.09	Quartz
			Sardinia (Italy)		
Miocene	Sinter	44.9	9.36	8.49	Quartz

Notes: The refined pseudo-Voigt coefficients describing the peak profile broadening of quartz (see text for details), and the mean crystallite size calculated from the Lorentzian part of the function using the Scherrer equation are also listed.

large size (100–200 μm) with respect to the average size of the quartz crystals observed in other SCT samples, although the well-developed grid-work texture is always present. These samples also show some pores between the quartz crystals, which are invariably absent in samples from other occurrences. The sub-perpendicular arrangement of elongated euhedral quartz crystals observed in the Gorno samples in SEM images is in agreement with optical investigations. SEM observations excluded the presence both of the "euhedral crystals of quartz developed as rosettes" characterizing the siliceous sinter deposits of Atiamuri and Umukuri in the Taupo Volcanic Zone of New Zealand (Herdianita et al. 2000) and the "interlocking mass of plate or sheet-like crystals" in the groundmass of the Magadi cherts (Schubel and Simonson 1990).

The Rietveld refined coefficients of the pseudo-Voigt function have been used to model the diffraction peak broadening of quartz (Larson and Von Dreele 1999). The resulting GW and LX parameters, representing the Gaussian and the Lorentzian part of the function, respectively (Table 2), show a remarkable consistency (mean values: <GW> = 12.0, <LX> = 3.81) in agreement with the optical microscopy observation that the quartz is well crystallized and relatively homogeneous in grain size in most of the SCT cherts. The average size of the coherently scattering domains, extracted from the refined Lorentzian coefficient by means of the Scherrer equation (Scherrer coefficient $K = 0.9$) is about 20.9 μm (Table 2), which

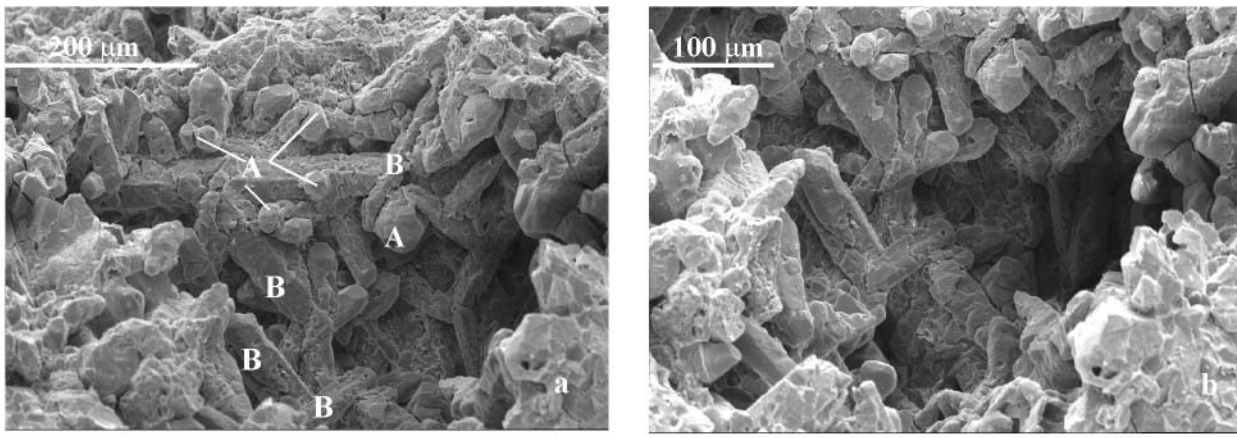

FIGURE 5. SEM images of the spatial relationship between quartz crystals in sample V2B. See text for labels A and B.

is in reasonable agreement with the mean grain size observed by optical microscopy. Only the samples from Calabria (TSA22) and the French Pyrenees (AS) show refined LX values slightly lower than average, and correspondingly they show a slightly larger mean crystallite size. As described before, this is interpreted to be a consequence of metamorphic recrystallization. Table 2 also reports for comparison the results of the Rietveld analysis of a Miocene quartz sinter sample from Sardinia: the refined peak profile parameters are more than twice those extracted from the SCT samples, and reflect a much smaller average crystallite size (about 8.5 μm), which is compatible with the values commonly reported for sedimentary cherts (Knauth 1994).

TEXTURE ANALYSIS, CORRELATION TO POLARIZED LIGHT MICROSCOPY AND SEM OBSERVATIONS

The textures of 11 samples associated with 5 different SCT occurrences, and 3 Pleistocenic Magadi-type cherts from the Lake Magadi area, Kenya, were quantitatively analyzed (Table 3). The SCT samples exhibit a moderate but marked texture, with a mean overall texture strength (F^2) of approximately 2. This texture strength is comparable to quartz textures developed in quartzites (Price 1985), granodiorites (Wenk and Pannetier 1990), and mylonites (Chateigner et al. 1999). As can be seen from the *R*P factors, all the orientation distributions were satisfactorily refined. The recalculated {001} and {100} pole figures of all the SCT samples are presented in Figure 6. Sample B1 exhibits all texture components and as such can be used to describe the textural features. The {001} pole figures, characterizing the distribution of *c* axes, exhibit two main components of orientation. The first component (labeled A in Table 2 and Fig. 6) is located about 35° from the normal to the surface of the sample. The second component (labeled B) is more inclined, from 60° to 85° from the normal, and distributed on a girdle. The 001 poles of component A show a maximum density of approximately 6.7 m.r.d. in sample BERC, and a minimum of about 1.7 m.r.d. for sample SL1 (Table 3). This 001 component corresponds to localized poles in the 100 pole figures, distributed around the expected pole for a single crystal, at 60° from one another and up to 35° from the equatorial

TABLE 3. Results of the texture analysis performed on SCT quartz samples from different localities

Occurrence	Sample	RP_0	RP_1	OD min	OD max	F^2	m.r.d. max in 001 pole figure	Textural components
Gorno District	PRAA	3.85	3.89	0.10	9.14	1.23	1.55	A-B
	PRA	5.64	5.09	0	16.86	1.63	2.76	A – B
	V2B	11.31	9.06	0	31.67	2.60	3.49	B
Palaeocarnic Chain	B1	11.34	8.25	0	33.39	3.08	2.85	A – B
	T11A	3.02	3.00	0.09	7.72	1.27	1.69	A – B
	T11A2	3.86	3.36	0	16.47	1.64	2.24	A – B
	T11B	3.77	3.51	0.11	8.84	1.24	2.07	A – B
	T25IA	6.20	5.96	0.03	32.04	1.88	2.34	A – B
Western Asturias	BERC	6.02	6.33	0	114.04	2.50	6.67	A
Hunan Province	XIK	5.12	5.12	0	38.15	3.01	2.83	A
Sardinia	SL1	4.05	3.94	0.08	9.17	1.33	1.66	A – B
Lake Magadi	MAG2	3.73	3.20	0.21	4.03	1.09	1.56	Low texture
	MAG3	3.16	2.97	0.35	2.80	1.05	1.47	Low texture
	MAG4	6.60	5.47	0.01	9.47	1.43	1.79	Low texture

Notes: The Lake Magadi cherts were analyzed for comparison.

plane. This component of orientation is due to quartz grains cut sub-perpendicularly with respect to the *c* axis, which remain almost constantly extinct under the microscope (i.e., red with the gypsum plate inserted: Figs. 4a–4c) upon sample rotation.

The second orientation component (B) is related to quartz crystals having *c* axes oriented about 75° from the normal to the surface of the sample (Fig. 6). The {001} poles for this component are distributed on a girdle which defines a fiber-like texture with a fiber axis inclined approximately 30° from the normal to the sample surface. Looking at the {100} pole figure, the fiber axis is aligned with <100> crystal directions. The girdle reinforcements, and the variations in A/B ratio among the samples, are mainly due to the contribution of larger grains, statistically not significant in the X-ray irradiated volume, as is shown by the neutron texture analysis. This second component corresponds to the quartz crystals appearing blue or yellow upon rotation of the microscope stage (Figs. 4a–4c) and are cut sub-longitudinally with respect to the *c* axis. The two orientation components A and B may be also recognized in the SEM images (Fig. 5): the orientation component A is represented by the small crystals (labeled A) that show a sub-hexagonal shape, while the orientation component B is represented by the elongated crystals (labeled B).

As mentioned previously, the texture components A and B do not change if we analyze parallel sections cut at different locations in the bulk specimen, and therefore they represent a truly three-dimensional feature of the investigated microcrystalline quartz samples. For instance, analyses T11A and T11A1 were performed on surfaces parallel to the macroscopic lamination of sample T11. Their textural features, represented by the {001} pole figures, are similar (Fig. 6), and show both A and B components. More surprisingly, analysis T11B performed on a surface perpendicular to the lamination of sample T11, mainly shows the A component of the {001} pattern. In fact, if the texture is homogeneous over the whole volume of the sample (but dispersed around its main components), *c* axes that are aligned close to the normal of a face will appear parallel to a perpendicular face, and vice-versa. This explains why in our case similar texture patterns are observed on perpendicular faces.

To verify the three dimensional character of the textures, we analyzed samples B1 and T11, cut into 1 cm edge cubes (Table 4), with neutrons (Fig. 7). The number of grains analyzed is much larger than for the X-ray experiments. The B components of the texture are located approximately in the equatorial plane, while the A component is absent. However, the maximum value for the B component is off the equatorial plane (80° from the normal to the sample, see crosses on Fig. 7), and its distribution clearly does not form a perfect fiber texture. This distribution covers the range of sub-perpendicular grains observed at local scale using X-rays and, associated with the presence of larger grains, may explain the appearance of the A component in the X-ray pole figures, which smoothes out when a larger number of grains is taken into account (as in neutron experiments). This observation corresponds with the X-ray analyses as seen in Figure 6, which shows the grainy appearance of X-ray pole figures for samples T11 and B1.

An interesting feature of the SCT quartz is the {101} pole figure (Fig. 8) which shows a crossed pattern which correlates to the orientation of the elongated crystals seen in polarized light microscopy. This typical feature of the pole figure may serve as an indicator of the SCT microstructure.

TABLE 4. Results of the texture analysis performed on samples B1 and T11 using neutron diffraction

Sample	RP_0	RP_1	OD min	OD max	F^2	m.r.d. max in 001 pole figure
B1	2.18	1.94	0.32	1.87	1.04	1.12
T11 quartz	2.76	2.79	0.52	1.53	1.02	1.27
T11 calcite	3.06	2.92	0.27	2.64	1.07	1.12

The samples of microcrystalline quartz of Magadi-type cherts that were analyzed for reference purpose generally show a nearly random texture with lower texture strengths (mean F^2 = 1.2 m.r.d.^{2}) than the SCT samples (Table 3). In the {001} pole figure (Fig. 9) of MAG4 it is possible to identify broad orientation maxima, when compared to the SCT samples, and correlatively lower densities (1.8 m.r.d.). The texture patterns are possibly associated with a grid-work texture, but it is much less pronounced, and has a broader azimuthal distribution. This indicates that, even in the presence of similar grid-work texture, the correlation between crystal axes and crystal morphology may be different.

The neutron {001} pole figures of calcite from sample T11 excludes the presence of orientational relationship between coexisting quartz and calcite, in agreement with the optical observations (Fig. 4d).

DISCUSSION

This study shows that SCT horizons are invariably composed of microcrystalline quartz exhibiting a three-dimensional grid-work texture. This peculiar texture is composed of two orientation components relative to the *c* axes of the quartz crystals, a principal component at approximately 35° from the normal to the surface of the sample and a second component oriented about 75° from the normal to the sample surface.

The formational processes must be interpreted within the framework of the geological constraints of the SCT horizons. As discussed previously, the grid-work texture of the SCT horizons is readily cancelled by relatively low-grade metamorphic processes. Therefore it may be assumed that the textures formed occurred under the typically low *P* and *T* conditions that characterize sedimentary environments, similar to those involved in the formation of cherts nodules hosted in epicontinental carbonate rocks, which lack any developed texture. The SCT quartz may be associated with a high rate of nucleation and/or to high SiO_2 activity. Because of the geological, mineralogical, geochemical, and textural constraints, the SCT horizons are considered to be distinct from other types of silica deposits in sedimentary environments (i.e., epithermal sinter, biogenic cherts, abiogenic lacustrine cherts, silcretes; see Hesse 1989 and Knauth 1994 for comprehensive reviews).

Although Magadi-type cherts, which are Pleistocene in age, also exhibit quartz textures and fast depositional processes, it is virtually impossible to extrapolate their sedimentary environments (highly alkaline lakes with pH > 10) to the

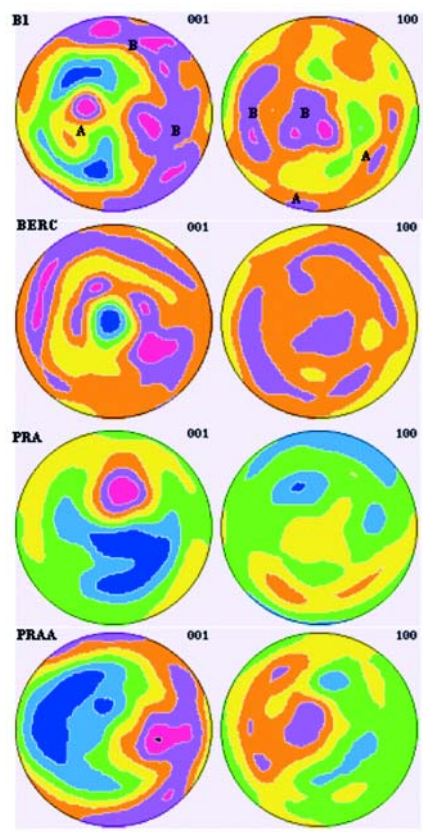

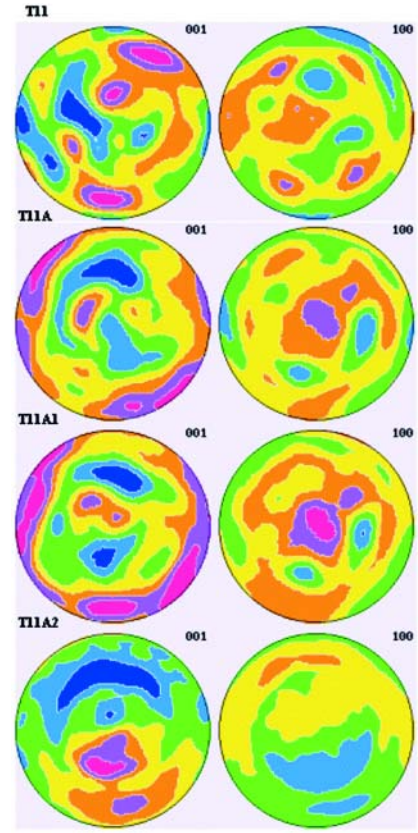

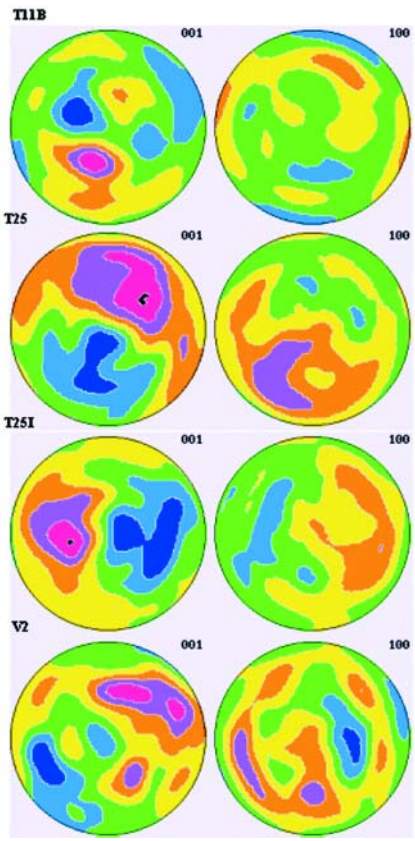

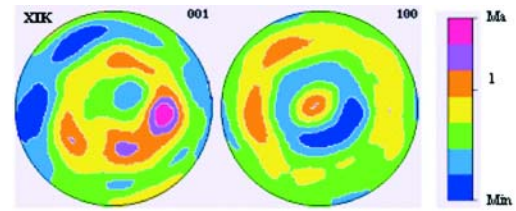

FIGURE 6. Recalculated {001} and {100} pole figures of all SCT samples. Texture components A and B are indicated for sample B1. Linear density scale, stereographic projection. Maxima are given in Table 2, minimum is 0.6 m.r.d.

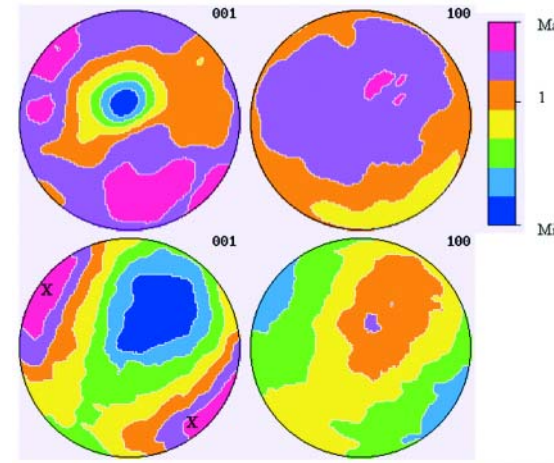

FIGURE 7. {001} and {100} pole figures of samples B1 (top row: maximum = 1.17 m.r.d., minimum = 0.6 m.r.d.) and T11 (bottom row: maximum = 1.27 m.r.d., minimum = 0.77 m.r.d.), recalculated from neutron diffraction experiments. Crosses indicate maxima of the {001} pole figure. Linear density scale, stereographic projection.

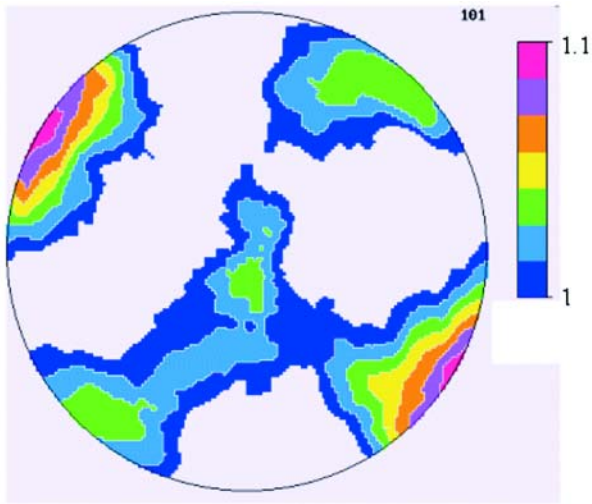

FIGURE 8. The {101} pole figure of T11 as recalculated from the ODF refined from neutron diffraction data. Note the crossed character of this pattern, strongly linked to crystal orientations observed by polarized light microscopy on SCT samples. Linear density scale, stereographic projection. Low level density has been removed for clarity.

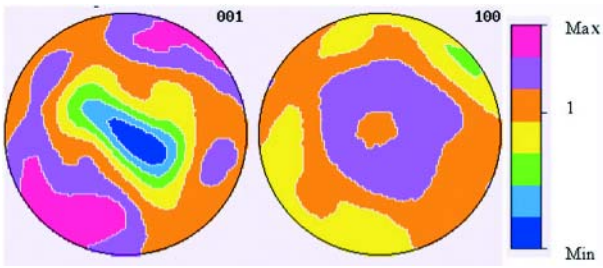

FIGURE 9. Recalculated 001 and 100 pole figures for the MAG4 sample, showing the relatively smooth texture compared to the SCT samples (Fig. 6).

palaeoenvironment envisaged for SCT horizons. Furthermore, the measured range of $\delta^{18}O_{SMOW}$ values of microcrystalline quartz in SCT horizons (+17–24‰, Camana 1999) is distinct when compared to the reported range of $\delta^{18}O_{SMOW}$ values for Magadi-type cherts (+32–44‰, O'Neil and Hay 1973) and the range of values reported for exhalative quartz sinters (+8–13‰, Ewers 1991).

The mechanism of formation of the grid-work texture in SCT cherts therefore must exclude both the oriented pressure components active in the formation of quartzite textures (Wenk 1998) and the processes invoked for the formation of Magadi-type cherts, whether biologically controlled, (Behr and Röhricht 2000), or inorganically controlled by spontaneous crystallization of SiO_2 (Hay 1968), or by magadiite transformation (Eugster 1967, 1969).

We tentatively support a model involving the nucleation of quartz seeds on the morphological faces of other developing quartz crystals. The angles (approximately 75° and 35°) observed in the 001 pole figures are quite consistent with crystals nucleating with the *c* axis perpendicular to some of the morphological faces that are most commonly developed in quartz, such as the prism $m\{100\}$, the positive and negative rhombohedra $r\{101\}$ and $z\{011\}$, and the rhombohedra that occur in the same zone as $r\{101\}$, such as $M\{301\}$ and Y{401} (Frondel 1962). All of these forms are listed as universal or very common forms of quartz. Some of the interfacial angles of interest are: [001] *Λ [301]* = 75.30°, [001] *Λ [401]* = 78.87°, [101] *Λ [011]* = 76.42°, and [100] *Λ [101]* = 38.21°. This mechanism does not require large chemical, temperature, or pressure gradients and it may therefore be consistent with the observed three-dimensionality of the grid-work textural and the homogeneous spatial distribution of the texture components in the samples.

The proposed mechanism may be applied as well to minerals other than quartz, and indeed there are examples in the literature where similar textures have been observed in rocks. One striking case is the so called "stellate" texture of calcite observed in the carbonatic cement matrix of Permian hiatus beds (Wetzel and Allia 2000) and other carbonates (Roberts et al. 1993).

ACKNOWLEDGMENTS

Financial support to G.A. is acknowledged from Italian MURST, Cofin projects. K.A. Schubel (Department of Geological Sciences, Binghamton University, New York) and H.J. Behr (Dept. of Geology, Göttingen) kindly made chert samples from Lake Magadi, Kenya available for this study. H.J. Behr is also thanked for sending us a copy of his recent work on Magadi cherts prior to publication.

REFERENCES CITED

Assereto, R., Jadoul, F., and Omenetto, P. (1977) Stratigrafia e metallogenesi del settore occidentale del distretto a Pb, Zn, fluorite e barite di Gorno (Alpi Bergamasche). Rivista Italiana di Paleontologia, 83, 3, 395–532.

Bechstädt, T., Boni, M., and Laske R. (1994) Sedimentological, stratigraphical and ore deposits field guide of the Autochtonus Cambro-Ordovician of South Western Sardinia. Memorie Descrittive Carta Geologica d'Italia, 48, I and II, 434 pp.

Behr, H.-J. and Röhricht, C. (2000) Record of seismotectonic events in siliceous cyanobacterial sediments (Magadi cherts), Lake Magadi, Kenya. International Journal of Earth Sciences, 89, 268–283.

Bonardi, G., De Vivo, B., Giunta, G., Lima, A., Perrone, V., and Zuppetta, A. (1982) Mineralizzazioni dell'arco Calabro-Peloritano. Ipotesi genetiche e quadro evolutivo. Bollettino Società Geologica Italiana, 101, 141–155.

Brigo, L., Dulski, P., Möller, P., Schneider, H.-J., and Wolter, R. (1988) Strata-bound mineralizations in the Carnic Alps/Italy. In J. Boissonnas and P. Omenetto, Eds., Mineral deposits within the European Community, p. 485–498. Springer Verlag, Berlin,

Brigo, L., Camana, G., Rodeghiero, F., and Potenza, R. (2001) Carbonate-hosted siliceous crust type mineralization of Carnic Alps (Italy-Austria). Ore Geology Reviews, 17, 199–214.

Bunge, H.-J. (1982) Texture analysis in materials science. (P.R. Morris Trans.) Butterworths, London.

Camana, G. (1999) Caratterizzazione mineralogica, chimica e geochimica di orizzonti silicizzati e mineralizzati legati a rocce carbonatiche: modellizzazione spazio-temporale e significato stratigrafico-sequenziale. Ph.D. Thesis, 182 p., Università di Milano.

———(2000) Mineralogical, chemical and geochemical characterization of silicified and mineralised horizons linked to carbonate rocks: spatial and temporal modelling and their significance in sequence stratigraphy. Plinius, 23, 49–53.

Camana, G., Artioli, G., and Chateigner, D. (2001) Different analytical approaches to the microstructure of a microcrystalline quartz. FIST, Geoitalia 2001, Chieti, 755–756.

Chateigner D., Wenk H.-R., and Pernet M. (1997) Orientation analysis of bulk YBCO from incomplete neutron diffraction data. Journal of Applied Crystallography, 30, 43–48.

———(1999) Orientation Distributions of low symmetry polyphase materials using neutron diffraction data: application to a rock composed of quartz, biotite, and felspar. Textures and Microstructures, 33, 35–43.

Eugster, H.P. (1967) Hydrous sodium silicates from Lake Magadi, Kenya; Precursors of bedded cherts. Science, 157, 1177–1180.

———(1969) Inorganic bedded cherts from the Magadi area, Kenya. Contribu-

tions to Mineralogy and Petrology, 22, 1–31.
Ewers, G.R. (1991) Oxygen isotopes and the recognition of siliceous sinters in epithermal ore deposits. Economic Geology, 86, 173–178.
Frondel, C. (1962) The system of mineralogy. Seventh edition. Vol. III, Silica Minerals, p. 36–75. Wiley, New York.
Hattori, I., Umeda, M., Nakagawa, T., and Yamamoto, H. (1996) From chalcedonic chert to quartz chert: diagenesis of chert hosted in a Miocene volcanic-sedimentary succession, central Japan. Journal of Sedimentary Research, 66, 163–174.
Hay, R.C. (1968) Chert and its sodium-silicate precursors in sodium-carbonate lakes of East Africa. Contributions to Mineralogy and Petrology, 17, 225–274.
Heizmann, J.-J. and Laruelle, C. (1986) Simultaneous measurement of several X-ray pole figures. Journal of Applied Crystallography, 19, 467–472.
Herdianita, N.R., Brown, P.R.L., Rodgers, K.A., and Campbell, K.A. (2000) Mineralogical and textural changes accompanying ageing of silica sinter. Mineralium Deposita, 35, 48–62.
Hesse, R. (1989) Silica Diagenesis: Origin of Inorganic and Replacement Cherts. Earth-Science Reviews, 26, 253–284.
Isoli, I. (1972) Le mineralizzazioni a fluorite nella Dolomia Principale norica in località Cammissinone nel comune di Zogno (Bergamo). Atti Società Scienze Naturali Museo Civico Storia Naturale Milano, 113, 63–88 .
Jadoul, F. and De Bonis, A. (1981) Paleogeografia e assetto strutturale delle mineralizzazioni a fluorite nella Dolomia Principale delle Prealpi Bergamasche. L'Industria Mineraria, 1, 19–34.
Jadoul, F., Bailo, F., and Pezzotta, F. (1993) Note su manifestazioni a fluorite, barite e celestina nelle successioni del Norico delle Prealpi Bergamasche. Bollettino Società Geologica Italiana, 112, 219–223.
Knauth, L.P. (1994) Petrogenesis of Chert. In P.J. Heaney, C.T. Prewitt, and G.V. Gibbs Eds., Silica: Physical behavior, geochemistry and materials applications, 29, 233–258. Reviews in Mineralogy, Mineralogical Society of America, Washington, D.C.
Krainer, K. and Spötl, C. (1998) Abiogenic silica layers within a fluvio-lacustrine succession, Bolzano Volcanic Complex, northern Italy: a Permian analogue for Magadi-type cherts? Sedimentology, 45, 489–505.
Larson, A.C. and Von Dreele R.B. (1999) GSAS, Generalized Structure Analysis System. Los Alamos National Laboratory, document LAUR 86–748.
Lovering, T.G. and Heyl, A.V. (1980) Jasperoids of the Pando Area, Eagle County, Colorado. U.S. Geological Survey Bulletin, 1474, 36 p.
Magliola-Mundet, H. (1972a) Contexto geológico de los yacimientos de fluorita de Musquiz, Estado de Coahuila, México. Boletin Geológico y Minero, 83-I, 48–67.
———(1972b) Généralisation d'un contrôle stratigraphique des gisements de fluorine du Nord de l'Etat de Coahuila, Mexique. Compte Rendu Academie des Sciences, Paris, 274, 3164–3167.
Matthies, S. and Vinel, G.W. (1982a) On the reproduction of the orientation distribution function of texturized samples from reduced pole figures using the conception of a conditional ghost correction. Physica Status Solidi, B 112, K111–K114.
———(1982b) An example demonstrating a new reproduction method of the ODF of texturized samples from reduced pole figures. Physica Status Solidi, B 112, K114–K120.
Matthies, S., Vinel, G.W., and Helming, K. (1987) Standard distributions in texture analysis. Akademie-Verlag, Berlin.
McNight, E.T. and Fischer, R. (1970) Geology and Ore Deposits of the Picher Field Oklahoma and Kansas. Geological Survey Professional Paper, 489, 109 p.
O'Neil, J.R. and Hay, R.L. (1973) $^{18}O/^{16}O$ ratios in cherts associated with the saline lake deposits of East Africa. Earth Planetary Science Letters, 19, 257–266.
Pouit, G. (1993) Les horizons minéralisés en Zn-Pb (Ba) du Paléoezoique des Pyrénées Centrales Françaises. Chroniques des Recherches Mineraires, 511, 21–31.
Pouit, G. and Bois, J.P. (1986) Arrens Zn (Pb), Ba Devonian deposit, Pyrénées, France: an exhalative-sedimentary-type deposit similar to Meggen. Mineralium Deposita, 21, 181–189.
Pretti, S. and Tamburrini, D. (1968) Le mineralizzazioni a barite della zona di Corona Sa Craba e Serra Lurdagu (Sulcis-Sardegna). Resoconti Associazione Mineraria Sarda, 6, 47 p.
Price, G.P. (1985) Preferred orientations in quartzites. In H.R. Wenk Ed., Preferred orientation in deformed metals and rocks: an introduction to modern texture analysis, p. 385–405. Academic Press, New York.
Ricote, J., Chateigner, D., Pardo, L., Algueró, M., Mendiola, J., and Calzada, M.L. (2000) Quantitative analysis of preferential orientation components of ferroelectric thin films. Ferroelectrics, 241, 167–174.
Roberts, H.H., Aharon, P., and Walsh, M.M. (1993) Cold-seep carbonates of the Louisiana continental slope-to-basin floor. In R. Rezak and D.L. Lavoie, Eds., Carbonate Microfabrics, Frontiers in Sedimentary Geology, 6, 95–104. Springer-Verlag, Berlin.
Robertson, J.F. (1963) Geology of the lead-zinc deposits in the Municipio de Januaria, State of Minas Gerais, Brazil. United States Geological Survey Bulletin, Reston, 1110-B, 35–110.
Rodeghiero, F. (1977) Le mineralizzazioni a Pb-Zn, fluorite, barite nel Carnico della zona del Pizzo della Presolana (Prealpi Bergamasche). Associazione Mineralogica Subalpina, 3-4, 453–474.
Rodeghiero, F. and Camana, G. (1999) Contrasting metallogenesis of ore districts of the Italian Alps. In C.J. Stanley et al., Eds., Mineral Deposits: Processes to processing, SGA-IAGOD International Meeting, London, 2, 897–900.
Rodeghiero, F., Fanlo, I., Subías, I., Fernandez-Nieto, C., and Brigo, L. (1996) Sulfide-, fluorite-, barite-bearing siliceous "crusts" related to unconformity surfaces of different ages in Pyrenees and Alps: a new, contrasting model for MVT deposits? Acta Geologica Hispanica, 30, 69–81.
Schönlaub, H.P. and Kreutzer, L.H. (1993) Lower Carboniferous Conodonts from the Cima di Plotta Section (Carnic Alps, Italy). Jahrbuch der Geologischen Bundesanstalt, 136, 1, 247–269.
Schubel, K.A. and Simonson, B.M. (1990) Petrography and diagenesis of cherts from Lake Magadi, Kenya. Journal of Sedimentary Petrology, 60, 761–776.
Souza de, S.L., Brito, P.C.R., and Silva, R.W.S. (1993) Estratigrafia, sedimentologia e recursos minerais da Formação Salitre na Bacia de Irecê, Bahia. CBPM, Serie Arquivos Abertos, 2, 24 p.
Spiro, B., Kim, A., and Tornos, F. (1999) Organic geochemistry and fluid inclusions of a fluorite deposit, Asturias, Spain. In C.J. Stanley et al., Eds., Mineral Deposits: Processes to processing, SGA-IAGOD International Meeting, London, 1, 279–282.
Subías, I. and Fernández-Nieto, C. (1995) Hydrothermal events in the Valle de Tena (Spanish Western Pyrenees) as evidenced by fluid inclusions and trace-elements distribution from fluorite deposits. Chemical Geology, 124, 267–282.
Subías, I., Recio, C., Fanlo, I., and Fernández-Nieto, C. (1997) Stable isotope composition of F-Pb-Zn mineralization in the Valle de Tena (Spanish Central Pyrenees). Mineralium Deposita, 32, 180–188.
Subías, I., Moritz, R., and Fernández-Nieto, C. (1998) Isotopic composition of strontium in the Valle de Tena (Spanish Central Pyrenees). Mineralium Deposita, 33, 416–424.
Subías, I., Fanlo, I., Yuste, A., Fernández-Nieto C. (1999) The Yenefrito Pb-Zn mine (Spanish Central Pyrenees): an example of superimposed metallogenetic events. Mineralium Deposita, 34, 220-223.
Tejerina, J.J. and Zorrilla, B.J. (1980) Descripcion geológica del distrito minero Caravia-Berbes (Asturias). Boletín Geológico y Minero, 91-6, 716–731.
Wenk, H.-R. (1998) Typical textures in geological materials and ceramics. In U.F. Kocks, C.N. Tomé, and H.R. Wenk, Eds., Texture and anisotropy–Preferred orientations in polycrystals and their effect on materials properties, p. 240–281. Cambridge University Press, U.K.
Wenk, H.-R. and Pannetier, J. (1990). Texture development in deformed granodiorites from the Santa Rosa mylonite zone, southern California. Journal of Structural Geology, 12, 177–184.
Wenk, H.-R., Matthies, S., Donovan, J., and Chateigner, D. (1998) BEARTEX: A Windows based program for quantitative texture analysis. Journal of Applied Crystallography, 31, 262–269.
Wetzel, A. and Allia, V. (2000) The significance of hiatus beds in shallow-water mudstones: an example from the Middle Jurassic of Switzerland. Journal of Sedimentary Research, 70, 1, 170–180.
Yeh, H.W. and Savin, S.M. (1977) Mechanism of burial metamorphism of argillaceous sediments: 3. O-isotope evidence. Geological Society of America Bulletin, 88, 1321–1330.
Yi, J., Camana, G., and Brigo, L. (1999) Carbonate-hosted deposits of the siliceous crust type in Italy and China. SGA-IAGOD International Meeting, Mineral Deposits: Processes to processing – London, vol. 2, 917–920.

MANUSCRIPT RECEIVED JULY 24, 2001
MANUSCRIPT ACCEPTED APRIL 29, 2002
MANUSCRIPT HANDLED BY GRANT FERRIS